DOI: 10.1002/cphc.201000834

# Improved Temporal Resolution and Linked Hidden Markov Modeling for Switchable Single-Molecule FRET

Stephan Uphoff, Kristofer Gryte, Geraint Evans, and Achillefs N. Kapanidis*[a]

Switchable FRET is the combination of single-molecule Förster resonance energy transfer (smFRET) with photoswitching, the reversible activation and deactivation of fluorophores by light. By photoswitching, multiple donor–acceptor fluorophore pairs can be probed sequentially, thus allowing observation of multiple distances within a single immobilized molecule. Control of the photoinduced switching rates permits adjustment of the temporal resolution of switchable FRET over a wide range of timescales, thereby facilitating application to various dynamical biological systems. We show that fast total internal reflection (TIRF) microscopy can achieve measurements of two FRET pairs with 10 ms temporal resolution within less than 2 s. The concept of switchable FRET is also compatible with confocal microscopy on immobilized molecules, providing better data quality at high temporal resolution. To identify states and extract their transitions from switchable FRET time traces, we also develop linked hidden Markov modeling (HMM) of both FRET and donor–acceptor stoichiometry. Linked HMM successfully identifies transient states in the two-dimensional FRET–stoichiometry space and reconstructs their connectivity network. Improved temporal resolution and novel data analysis make switchable FRET a valuable tool in molecular and structural biology.

## 1. Introduction

The function of biomolecules is closely linked to their structure. Performing structural studies on single molecules allows the observation of heterogeneity between molecules,[1–3] such as structural differences between static or slowly interconverting molecular subpopulations[4] or dynamic heterogeneity associated with structural changes[5] and transient molecular interactions.[6] The fundamental role of heterogeneity in biological systems[7] demands methods that maximize information from individual molecules. Fluorescence techniques have unique properties in this context, owing to labeling specificity and instrumentation that allows detection of single fluorophores even in complex environments such as living cells. In particular, single-molecule Förster resonance energy transfer (smFRET) is widely used to probe biomolecular structure and dynamics by exploiting the distance dependence of the dipole–dipole interaction between a donor and an acceptor fluorophore.[8–11] Formation of detailed structural models or complex reaction pathways requires multiple FRET measurements with donors and acceptors attached at different positions.[12–15] Yet, combining information from different measurements on heterogeneous systems is not straightforward; to address this challenge, multicolor FRET methods have been developed that monitor multiple FRET pairs per molecule.[16,17] Moreover, improved understanding and control of photophysics enables uninterrupted measurements of single immobilized organic fluorophores over minutes,[18,19] permitting direct, real-time observation of dynamic heterogeneity, for example, reaction cycles and nonequilibrium processes.[20–22]

By exploiting rather than suppressing specific photophysical properties of organic fluorophores, we have recently introduced "switchable FRET" as a tool in molecular and structural biology.[23] Switchable FRET combines photoswitching and smFRET to probe sequentially multiple donor–acceptor pairs within an individual molecule. Photoswitching is the controlled deactivation and activation of fluorophores by light[24–26]—a process central to super-resolution microscopy.[27–29] In switchable FRET, photoswitching separates temporally the FRET interaction of different acceptors with a shared donor. Considering technical and conceptual limitations of multicolor FRET techniques,[30,31] switchable FRET should be a useful addition to the toolbox for probing structure and dynamics of individual molecules from more than one perspective, especially in heterogeneous systems (Figure 1).

Herein we report optimized photoswitching conditions of cyanine fluorophore Cy5 for switchable-FRET applications; the new conditions increase the temporal resolution of the method by more than an order of magnitude, provide tunability over a wide range of timescales, and open applications to processes occurring on the subsecond timescale. In addition to total internal reflection (TIRF) microscopy, we show that switchable FRET is also compatible with confocal microscopy. Finally, we lay out how linked hidden Markov modeling (linked HMM) provides a powerful way of identifying states in two-dimensional time traces and extracting their connectivity network. These extensions of switchable FRET significantly improve its capabilities with regard to the study of complex heterogeneous biological systems.

[a] S. Uphoff, K. Gryte, G. Evans, Dr. A. N. Kapanidis
Department of Physics and Biological Physics Research Group
University of Oxford, Parks Road, Oxford OX1 3PU (UK)
Fax: (+44) 1865-272-400
E-mail: a.kapanidis1@physics.ox.ac.uk

  

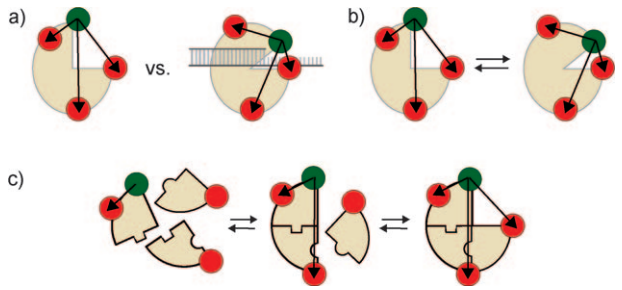


**Figure 1.** Multiple FRET pairs provide insight into heterogeneous biological systems from multiple perspectives. a) Static structural heterogeneity; for example, distinct protein conformations in a ligand-bound and free form. b) Dynamic structural heterogeneity; for example, conformational fluctuations associated with enzymatic function. c) Dynamic and static structural heterogeneity; for example, transient formation and dissociation of multimolecular complexes.

## 2. Results and Discussion

### 2.1. Periodic Photoswitching

The concept of probing different FRET acceptors over time by using photoswitching can, in principle, be realized in two ways, either in a periodic or stochastic manner; we demonstrated the latter previously.[23] Here we first explored periodic photoswitching of Cy5, a popular cyanine fluorophore for super-resolution microscopy and smFRET spectroscopy; Cy5 can be photoswitched by cycling red and green excitation.[24,25] In each cycle of periodic switchable FRET, red excitation switches all acceptors off, after which green excitation activates a single acceptor and probes its particular FRET efficiency. Different acceptors can thus be measured by sequential cycling.

Using TIRF microscopy, we studied immobilized dsDNA molecules, each labeled with a single Cy5 acceptor separated by ten base pairs (bp) from a Cy3B donor. Cycles of 9 s red excitation and 1 s green excitation at 1 mW intensity reversibly switched the majority of Cy5 molecules on and off (Figure 2a). Deactivation was very slow compared to activation, the latter occurring almost instantaneously for all acceptors during green excitation intervals (green highlighted segments, Figure 2a). Irreversible photobleaching is apparent from the gradual decay of the peak numbers of molecules in each cycle (ca. 250 molecules at 5 s; ca. 130 molecules at 85 s). The fluorescence time trace of a single Cy5 from the same data set shows a steplike appearance (ca. 600 counts/100 ms) and disappearance of fluorescence emission, a signal that clearly marks reversible photoswitching at the single-molecule level (Figure 2b). Most single Cy5 activation events coincide with the beginning of a green excitation pulse, during which we observed Cy5 fluorescence owing to FRET by the nearby Cy3B donor (ca. 250 counts/100 ms, green background). Thermal activation and residual green intensity during red excitation intervals induced a few stochastic activation events, which account for the offset of 40–50 active molecules in Figure 2a.

Probing different acceptors on one molecule sequentially requires activation rates to be tuned such that, on average, only a single acceptor is active during green excitation intervals. Here, green excitation provides the FRET signal but also leads to undesirable high activation rates. Considering the additional complication of the dependence of the Cy5 activation rate on its distance from the donor (described below), we conclude that periodic photoswitching with Cy5 is not practical for switchable FRET.

### 2.2. Switchable FRET by Stochastic Photoswitching

Previously, we realized that stochastic photoswitching can be used to separate active state intervals of multiple identical fluorophores attached to the same molecule in such a way that they can be interrogated individually over time.[23] In this work, we further explored this concept. We applied alternating-laser excitation (ALEX) at 532 and 635 nm (0.5 mW intensity) with a period of 200 ms, such that the alternation rate exceeded the activation and deactivation rates of Cy5. Under these conditions, individual Cy5 molecules showed reversible stochastic photoswitching, apparent from spontaneous transitions between a bright state and a dark state (Figure 2c).

Alternating-laser excitation also allowed continuous observation of the apparent FRET efficiency $E^*$ and the relative donor–acceptor stoichiometry $S$.[11] To this end, we split donor and acceptor fluorescence into two detection channels on an EMCCD camera,[20] extracting the following fluorescence signals $F_{AA}$ (Cy5 emission upon 635 nm excitation), $F_{DD}$ (Cy3B emission upon 532 nm excitation), and $F_{DA}$ (Cy5 emission upon 532 nm excitation). Using ratios of these signals we obtain $E^*$ and $S$; specifically, $E^* = F_{DA}/(F_{DD}+F_{DA})$ and $S = (F_{DD}+F_{DA})/(F_{DD}+F_{DA}+F_{AA})$. Active and inactive states of Cy5 in the presence of Cy3B display intermediate and high $S$ values, respectively, yielding distinct clusters in the $E^*$–$S$ histogram (Figure 2c, right). In agreement with the Förster radius of 6.7 nm for Cy3B and Cy5 in this sample,[23] their 10 bp (3.4 nm) separation led to a high FRET efficiency ($E^* \approx 0.8$). Residual nonzero FRET efficiency in the inactive state represents leakage of donor fluorescence into the acceptor detection channel.[32]

A different dsDNA construct with 19 bp separation between Cy3B and Cy5 also showed reversible stochastic photoswitching, but a lower FRET value of $E^* \approx 0.35$, corresponding to the larger donor–acceptor separation (Figure 2d). We observed that the inactive state of 19 bp Cy5 was more stable compared to the inactive state of 10 bp Cy5 under ALEX. In fact, photoactivation of Cy5 is not only induced by direct 532 nm excitation, but also by energy transfer of a nearby donor fluorophore. Photoactivation rates of a Cy5 acceptor in a switchable FRET experiment thereby depend on its distance to the donor fluorophore, as shown previously.[24]

We successfully applied stochastic photoswitching of two Cy5 acceptors to measure two different donor–acceptor distances within an individual molecule and applied this method to structural measurements on a protein–DNA complex and on dynamic DNA Holliday junctions.[23] Example data of dsDNA labeled with both Cy5 acceptors at 10 bp and 19 bp separation from one Cy3B donor are shown in Figure 3a. In addition to the donor-only state and the two states with either 19 bp Cy5 or 10 bp Cy5 active, we also observed the state with both Cy5

  

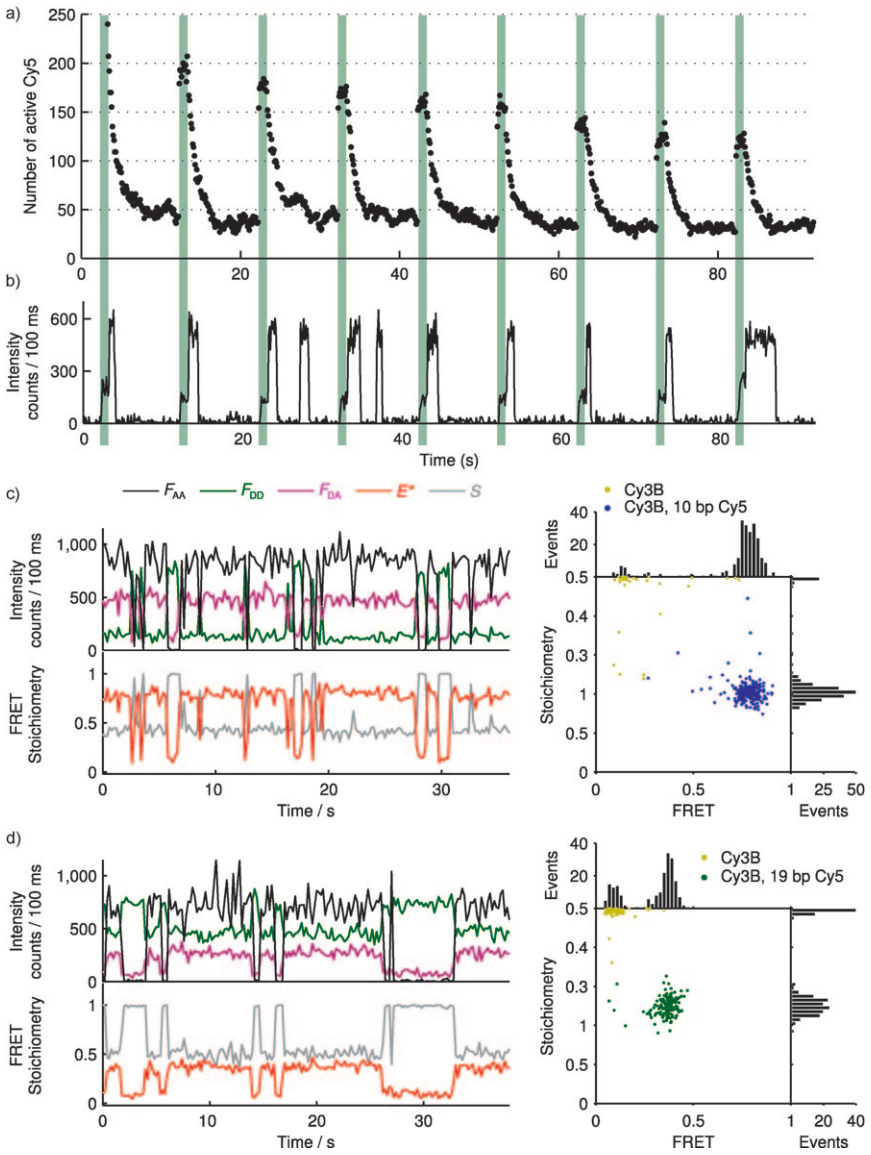


**Figure 2.** Reversible photoswitching of Cy5. a) Periodic switching. Immobilized dsDNA labeled with Cy5 and Cy3B at 10 bp separation was measured by cycles of 9 s excitation at 635 nm and 1 s excitation at 532 nm by using TIRF microscopy. Green background marks 532 nm excitation. A localization algorithm determined the number of active fluorescent Cy5 molecules in each 100 ms frame within a field of view. b) Fluorescence intensity–time trace of an individual Cy5 molecule from the sample in a). c–d) Stochastic photoswitching. ALEX for a 200 ms period by using TIRF microscopy induced stochastic and reversible photoswitching of Cy5 at c) 10 bp separation and d) 19 bp from Cy3B on immobilized dsDNA. Fluorescence intensities ($F_{AA}$, $F_{DD}$, and $F_{DA}$) are shown in the top graphs, corresponding FRET efficiency ($E^*$) and stoichiometry ($S$) versus time traces are plotted below. Data from individual time traces (left) were plotted on $E^*$–$S$ histograms for a single molecule (right). The two clusters in each histogram represent the active and the inactive acceptor state.

active at the same time at a low $S$ value. We note that absolute $S$ values depend on the relative excitation intensities at 532 and 635 nm, which explains shifts in $S$ between different experiments with different excitation intensities.

### 2.3. Buffer Conditions for Switchable FRET

Switchable FRET requires buffer conditions that induce photoswitching of acceptor fluorophores without perturbing stable donor fluorescence. To probe multiple acceptors over time, minimizing donor photobleaching is crucial. A standard enzymatic oxygen-scavenging system[33] plus β-mercaptoethanol (BME), a thiol-containing reducing agent, which drives photoswitching of Cy5 by forming a transient bond with the polymethine chain,[34] met these needs. In addition, BME acts as a triplet quencher to minimize photobleaching of organic fluorophores.[18]

We found, however, that Cy3B bleached within a few seconds of 532 nm excitation in freshly prepared switching buffer containing 14.3 mM BME, while reversible photoswitching of Cy5 was very efficient. In agreement with the mechanism by which Trolox serves as an antibleaching reagent,[35] we found that incubation of BME in solution at 37 °C for 24 h increased its performance as antibleaching reagent while preserving its function as an inducer of photoswitching; increased temperature accelerated this process. We also observed a gradual decrease in the deactivation rates of Cy5 upon storage of BME in solution at 4 °C for several months. We hypothesize that, during incubation, an oxidized form of BME is generated which quenches the triplet state by a combination of reduction and oxidation according to the ROXS principle,[19] thereby inhibiting photobleaching. The consumption of the reduced form of BME during incubation and storage explains the decreased deactivation rates of Cy5. We noticed a similar behavior for mercaptoethylamine.[23]

### 2.4. Fast Switchable FRET Using TIRF Microscopy

Activation and deactivation of Cy5 are photoinduced processes requiring population of excited states, and hence depend on the excitation intensity.[29] We used this property to "tune" the measurement time and temporal resolution of switchable FRET. Increased excitation intensities induced faster photoswitching, while the higher photon count rate permitted faster

  

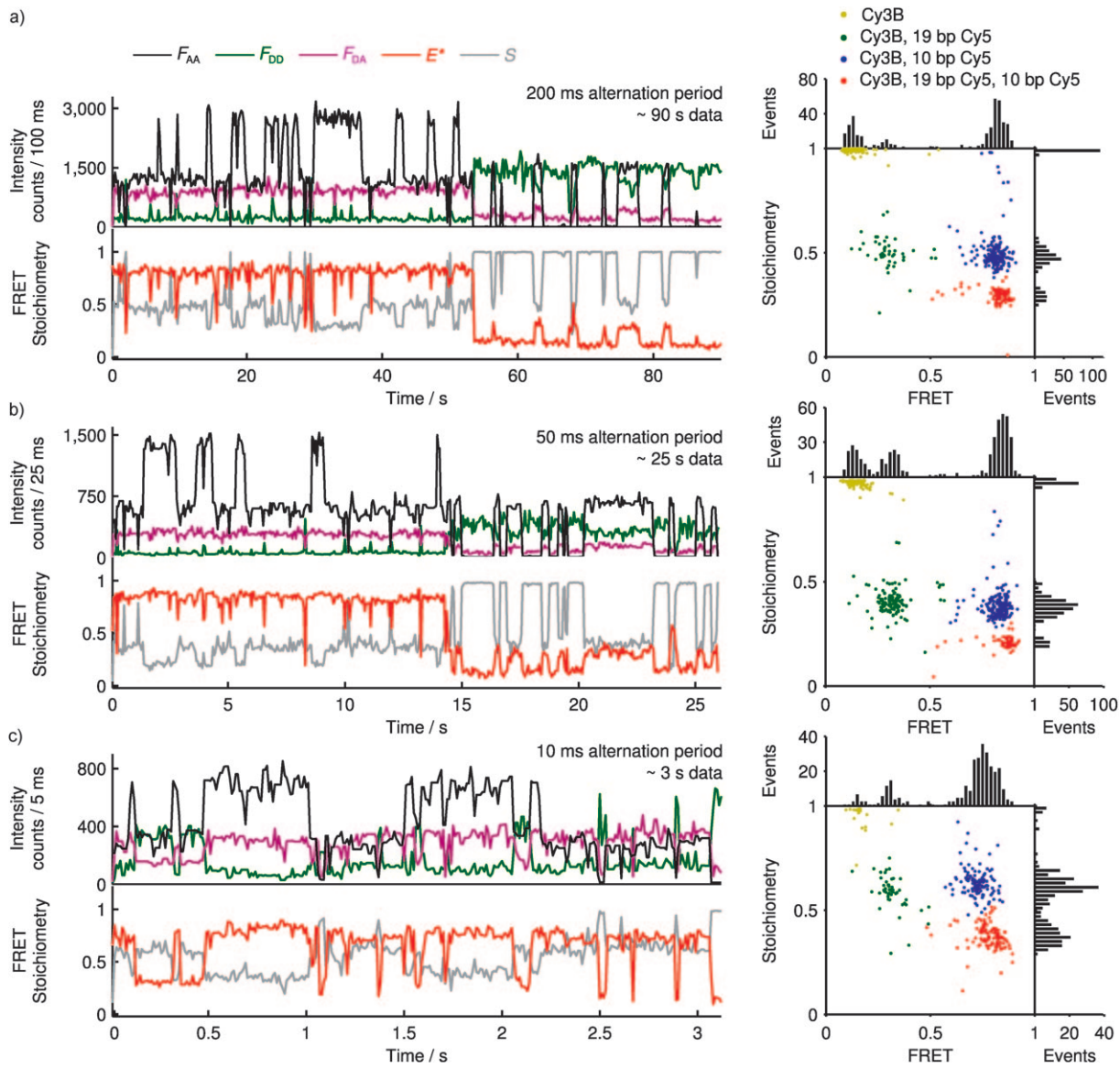


**Figure 3.** Switchable FRET with tunable temporal resolution. TIRF microscopy at different ALEX intensities and periods probed immobilized dsDNA labeled with Cy3B and two Cy5 at 10 and 19 bp separation. The laser alternation period equals the temporal resolution. Switching rates and temporal resolution increase from top to bottom. a) 200 ms alternation period, 1 mW green and 1 mW red excitation. b) 50 ms period, 2 mW green and 2 mW red excitation. c) 10 ms period, 4 mW green and 4 mW red excitation. *E**–*S* histograms (right) represent data of single-molecule time traces (left). The cluster at high *S* represents the Cy3B-only state; two clusters at intermediate *S* show high and low *E** of the proximal and distal Cy5; while the cluster at low S accounts for the state with both active Cy5.

laser alternation together with shorter camera exposure per frame. With little loss in data quantity and quality, measurement times could be adjusted from more than a minute down to about 1.5 s with corresponding temporal resolution of 200 ms down to 10 ms (Figure 3a–c). The camera readout rate became a limiting factor for data in Figure 3c, which was acquired by using 2×2 pixel binning and a reduced field of view.

The on/off time ratio significantly differed for the proximal and distal Cy5. Due to its lower ratio, the distal Cy5 was probed mostly after the proximal Cy5 photobleached irreversibly (as in Figure 3a,b). For this reason, distance-dependent activation rates limit the applicability of Cy5 as an acceptor in switchable FRET experiments with more than two acceptors. We previously tested photoswitchable acceptor ATTO655 in combination with Cy3B donor in switchable FRET experiments.[23] ATTO655 switches through a combination of reduction and oxidation reactions and did not exhibit distance-dependent activation rates; both acceptors had the same on/off time ratio and were probed stochastically over time. We note that a wide range of organic fluorophores that can be rendered photoswitchable is available[36] from which to choose the optimal fluorophore pair for switchable FRET experiments on a particular system.

Control of photoswitching rates is important for applying switchable FRET to various biological systems and processes. Examination of transient short-lived structural states from mul-

  

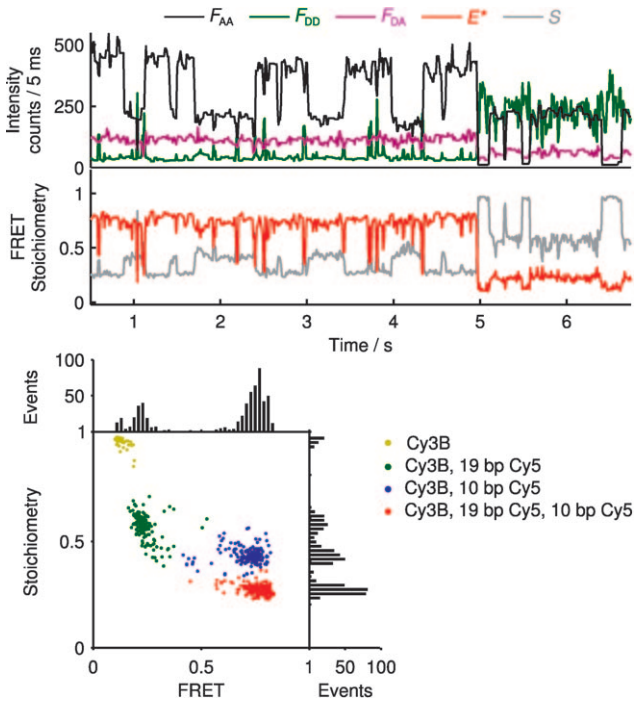


**Figure 4.** Switchable FRET by confocal microscopy. ALEX at 100 μs alternation period probed a single immobilized dsDNA molecule labeled with two Cy5 at 10 and 19 bp separation from one Cy3B. Displayed data were integrated at 10 ms resolution. Data representation as in Figure 3.

tiple perspectives needs sufficiently fast switching rates to record different acceptors during the dwell time of a state. On the other hand, observation of rare events requires long time traces of single molecules without photobleaching. Our results show that switchable FRET should be applicable to the whole range of biological processes to which conventional smFRET can be applied. Importantly, measuring more than two distances by switchable FRET will be facilitated by switching rates that generate a small on/off time ratio, so as to ensure that each acceptor is probed individually before irreversible photobleaching.

### 2.5. Fast Switchable FRET Using Confocal Microscopy

To further extend the dynamic range of switchable FRET and enable statistical photon trajectory analysis, we used confocal microscopy on surface-immobilized molecules.[37] Single immobilized molecules were located after scanning a field of view with a piezo stage, positioned at the center of the fixed laser excitation focus, and measured one at a time. We applied red (639 nm) and green (532 nm) ALEX at 100 μs period and recorded photon arrival times continuously in the spectrally separated donor and acceptor detection channels by avalanche photodiodes. For display, fluorescence counts were integrated at 10 ms temporal resolution (Figure 4). Switchable FRET experiments were performed under the same sample and buffer conditions as above.

Data quality for confocal microscopy was improved compared to high-temporal-resolution TIRF microscopy, while photobleaching and switching rates were similar. Focusing excitation onto a diffraction-limited spot centered on a single molecule gives high local excitation intensity and optimal signal-to-background ratio, but at the sacrifice of parallel acquisition of molecules provided by TIRF-based imaging (although microscopy formats with multiple confocal spots can also be used). While the frame rate for TIRF microscopy is currently limited to greater than 1 ms (due to camera readout rates), confocal scanning microscopy can achieve even higher temporal resolution before the fluorescence emission saturates at high excitation intensities. Compared to TIRF microscopy, no further image processing is needed in confocal microscopy. Combination of differences in quantum yield and detection efficiency of donor and acceptor caused the difference in $S$ between the low- and high-FRET states; the extent of this difference varies between microscopes with distinct filter sets and detectors.[32]

### 2.6. Hidden Markov Modeling of Switchable FRET Data

Switchable FRET reports on multiple FRET states originating from different acceptors per molecule. Data analysis is required to identify these states and extract information such as the mean $E^*$ and $S$ values. We analyzed data in Figures 3–5 using the standard clustering algorithm k-means, which assigns data points to clusters by minimizing the sum of distances to the corresponding centroid of their clusters in the $E^*$–$S$ histogram. This strategy relies on clear separation between clusters. Standard signal processing algorithms (such as moving median or frequency domain filters) fail to enhance the discontinuous stepping behavior characteristic of single-molecule time traces. Here, we applied a new step-filter method (l1-norm piecewise constant) to increase resolution of states.[38] This filter robustly approximates the data globally (as opposed to sliding-window algorithms) by a piecewise constant curve, given a single parameter $\lambda$. For small $\lambda$, the noisy time trace is reproduced closely, while the algorithm fits extended constant intervals with steplike transitions for larger $\lambda$ (here $\lambda = 2e{-}4$).

State finding by data clustering is not optimal, as it does not exploit the temporal information available from switchable FRET. Time traces contain the temporal sequence of discrete instantaneous switching events which mark transitions between states, each individual state being associated with both the number of active acceptors at any one time and the proximity of a given acceptor to the donor. In particular, the connectivity of states, that is, the network of transitions, can be highly useful to build kinetic models. Experimental noise, however, obscures the sequence of transitions. Recent literature suggests that hidden Markov model (HMM) analysis can be used to recover such underlying state sequences from noisy fluorescence trajectories, along with parameters related to the individual state variables.[39–43] Switchable FRET with its single-exponential switching kinetics lends itself quite readily to HMM analysis. After sampling the various HMM methods available, the vbFRET package developed by Bronson and co-workers[42] yielded the best results and was most amenable to our current

  

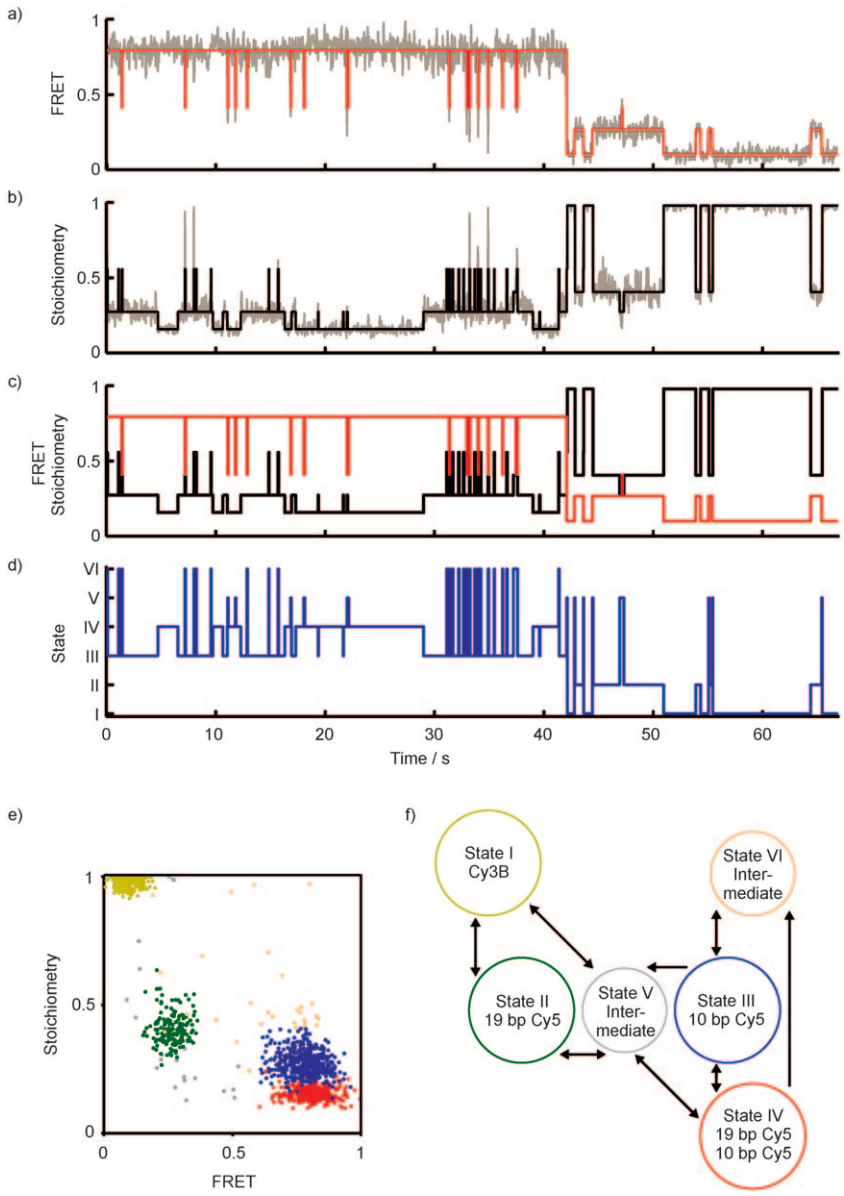


**Figure 5.** HMM analysis of switchable FRET data. a) One-dimensional HMM analysis on *E** time trace. Raw data in gray. b) One-dimensional HMM analysis on *S* time trace. Raw data in gray. c) Superposition of *E** and *S* HMM analysis. d) Linked state trajectory. e) Identified states in the *E**–*S* plot. f) Connectivity network of states. Direct state transitions detected in the data are shown as arrows.

MATLAB data analysis software. This package offers the additional advantage over other smFRET HMM implementations in that the algorithm used not only selects the most likely parameter values pertaining to the individual states, but also selects the most parsimonious model, thus avoiding the tendency of traditional maximum likelihood methods to "overfit" the data.[42]

Switchable FRET, however, poses a distinct problem, as FRET alone provides only partial information and is neither able to adequately comment on either fluorophore stoichiometry or photophysics nor able to explicitly delineate which acceptor is contributing to FRET at any one time. We developed linked HMM analysis of both *E** and *S* trajectories to resolve these shortcomings by temporally associating both FRET and stoichiometry information.[44] The concept of linked HMM analysis is illustrated on a representative time trace from experimental data (Figure 5). First, independent one-dimensional HMM analysis extracted state trajectories of *E** and *S* time traces (Figure 5a, b). Subsequently, these state trajectories were superimposed to form linked *E**–*S* states in a one-dimensional state trajectory (Figure 5c, d). A final round of HMM analysis on the linked state trajectory assigned states in the two-dimensional *E**–*S* space (Figure 5e) and extracted connectivity and kinetic information (Figure 5f).

Six states were identified in total. Linked HMM assigned four states as follows: I) donor-only (Cy3B), II) low-FRET (Cy3B, 19 bp Cy5), III) high-FRET (Cy3B, 10 bp Cy5), and IV) both active acceptors (Cy3B, 19 bp Cy5, 10 bp Cy5). Even though *E** of states III and IV were equal within noise, linked HMM combines *E** and *S* information to successfully separate them. Linked HMM assigned spurious data between clusters to two additional states (V, VI). Taking into account temporal information available from HMM, we found that states I–IV had dwell times on the order of 10–30 frames, while states V and VI lasted for about a single frame on average and account for less than 5% of the data. We interpret data of these states as intermediate values owing to switching events in combination with the finite integration time of the camera. These outliers typically perturb cluster analysis but were successfully isolated by using linked HMM.

The connectivity network provided additional information on the interconversion of states (Figure 5f). We found that most transitions involved one of the intermediate states, as expected. Directly observed transitions occurred between the donor-only state (I) and the low FRET state (II), as well as between the high FRET state (III) and the state with both active Cy5 (IV). Generally, direct transitions between states of different acceptors (e.g. from II to III) are "forbidden"; instead, such transitions must involve the donor-only state or states with multi-

  

ple active acceptors as intermediates. Similarly, we did not observe direct transitions between the donor-only state and multi-acceptor states.

We further validated the linked HMM algorithm using Monte Carlo simulation to generate $E^*$–$S$ time traces based on the data in Figure 5. For the majority of simulated time traces, linked HMM correctly identified four states and extracted the input $E^*$ and $S$ values with high accuracy (Table 1). Analysis of simulated time traces also uncovered a limitation of the current algorithm that infrequently confused the FRET values of state III ($E^*=0.79$) and state IV ($E^*=0.82$). This error occurred only for dwells shorter than seven frames in 24% of simulated time traces. For the remaining 76% of time traces, the simulated underlying state trajectory and the linked HMM trajectory agreed for 99.51% of frames.

**Table 1.** Linked HMM results for simulated data. Linked HMM state values found for each of the four $E^*$–$S$ states (simulation input values given in parenthesis). Details of simulation and linked HMM analysis are described in the Experimental Section.

| | $E^*$ | $S$ |
|---|---|---|
| State I (Cy3B-only) | 0.0999 (0.10) | 0.9804 (0.98) |
| State II (19 bp Cy5) | 0.2696 (0.27) | 0.3996 (0.40) |
| State III (10 bp Cy5) | 0.7900 (0.79) | 0.2690 (0.27) |
| State IV (19 bp Cy5, 10 bp Cy5) | 0.8194 (0.82) | 0.1526 (0.15) |

## 3. Conclusion

Development of advanced experimental techniques contributes significantly to rapid progress in the field of single-molecule biophysics.[45] Herein, we extended switchable FRET, a recently introduced method for probing multiple FRET pairs within an individual molecule. Enhanced control of photoswitching and compatibility with confocal microscopy allows application of the method on a wide range of time scales. In contrast to TIRF microscopy, confocal microscopy, as presented here or with pulsed excitation, records photon arrival times, a feature that could be used to combine switchable FRET with statistical correlation and fluctuation analysis, as well as photon-by-photon analysis.[46]

Similar to super-resolution techniques, the performance of switchable FRET depends primarily on controlled photoswitching. The number of FRET pairs measurable by switchable FRET is limited mainly by the width of FRET distributions,[47] provided that the on/off time ratio of each acceptor can be adjusted to be sufficiently small. Currently, this was not possible for Cy5 as a switchable acceptor, limiting the number of Cy5 acceptors to two. Considering the rapid development in super-resolution techniques, which also benefit from small on/off time ratios,[48] more suitable fluorophores and imaging conditions for switchable FRET should become available soon.

We applied a filtering algorithm to facilitate clustering of states. To use temporal information from switchable FRET time traces, we developed linked HMM analysis.[44] Our novel algorithm detects states in two-dimensional $E^*$–$S$ time traces and builds a connectivity network that shows the interconversion of states. The combination of state identification and kinetic information makes HMM a powerful data analysis tool, and along with ongoing developments in instrumentation and switchable fluorophores, it should help establish switchable FRET as a valuable tool for dynamic structural biology.

## Experimental Section

Sample Preparation and Single-Molecule Data Acquisition: Preparation of coverslips with immobilized dsDNA labeled with either (Figure 2) or both (Figure 3) Cy5 acceptors at 10 bp and 19 bp separation from one Cy3B donor, and data acquisition for TIRF microscopy were described previously.[23] Imaging was performed in switching buffer [10 mM Tris-HCl (pH 7.5), 10 mM NaCl, 14.3 mM β-mercaptoethanol (BME)] that was incubated at 37 °C for 24 h and stored at −20 °C. Oxygen was removed from the imaging buffer by adding 10% (w/v) glucose, 1 mg mL$^{-1}$ glucose oxidase, and 40 μg mL$^{-1}$ catalase directly before each experiment.

Confocal Scanning Microscopy: Data in Figure 4 were acquired with a custom-built epifluorescence confocal scanning microscope. Green (532 nm, MGL532, CNI) and red (639 nm, Power Tech. Inc.) lasers were spatially filtered and overlaid by using a single-mode angle polished fiber optic cable (PMC-460, Schäfter + Kirchhoff), collimated, and coupled into an objective (60× Water Immersion, Olympus) via a dichroic mirror (XF94 535/635TBDR, Omega). Fluorescence was collected and filtered by the same objective–dichroic pair, split into its green and red components (XF2021 630DRLP, Omega), further filtered (filters HQ 585BP70 and HQ 725BP110, Chroma), and focused onto avalanche photodiodes (SPCM-AQR-14 Photon Counting Module, Perkin-Elmer), with the finite APD detector area acting as the pinhole component (spatial filtering element). This simplification allowed for fewer optical components and a more compact microscope. Alternating-laser excitation at 10 kHz and measurement of photon arrival times were digitally controlled (PCI-6602 board, National Instruments). A piezoelectric scanning stage (P-733.2CD) with E-761 Digital Piezo Controller PCI board (Physik Instrumente) and custom-written LabVIEW software (National Instruments) were used to automatically locate single immobilized molecules. The microscope was built completely lightproof to allow measurement under ambient light conditions.

Data Filtering and Linked HMM Analysis: Prior to k-means clustering, data in Figures 3 and Figure 4 were processed by using the l1-norm piecewise constant step filter.[38] The algorithm minimizes two terms: the deviation of the solution from the input, and the difference between adjacent data points of the solution, which favors a steplike solution with piecewise constant intervals. The single fitting parameter, here $\lambda=2e{-}4$, describes the trade-off between the two minimizations. For $\lambda=0$, the data is reproduced exactly, whereas for larger $\lambda$ the fit tends towards a solution with pronounced piecewise constant intervals.

Hidden Markov model (HMM) analysis was used to exploit temporal information available from switchable FRET time traces. To identify states in the two-dimensional $E^*$–$S$ space, we developed linked HMM. The implemented algorithm, based on the vbFRET package,[42] proceeds as follows: 1) reiterative application of the forward–backward algorithm[49] generates a variational Bayes approximation of the model evidence (most likely number of states), as well as the model parameters (state transition probabilities, means, and precisions); 2) the Viterbi algorithm[50] determines the most probable hidden state trajectory from the most probable parame-

  

ters determined in step 1; 3) repetition of steps 1 and 2 finds the model with the highest evidence (maximum number of states supported by the data); 4) after independent HMM analysis of individual $E^*$ and $S$ time traces, linking the idealized $E^*$ and $S$ trajectories yields a metaspace trajectory $T$, where $T$ includes a subset of all possible state combinations $\{(E^*_1, S_1),..,(E^*_1, S_N),..,(E^*_M, S_1),..,(E^*_M, S_N)\}$ where $M$ and $N$ are the total number of $E^*$ states and $S$ states, respectively; 5) repetition of steps 1–3 on $T$ returns the underlying state sequence (donor–acceptor proximity and number of active acceptors) best supported by the data; 6) temporal segmentation of $T$ permits a) extraction of the linked $E^*$–$S$ state transition sequence, and thus generates a connectivity network showing pathways between individual states, and b) deconvolution into segmented $E^*$ and $S$ trajectories, revealing the association of individual $E^*$ and $S$ states. In this work, analysis was free to find anywhere from 1 to 10 states for the individual $E^*$ and $S$ trajectories and anywhere from 1 to the total number of $E^*$–$S$ combinations for $T$. All subsequent connectivity and parameter extraction pertained to the model with highest evidence.

Monte Carlo Simulation and Linked HMM Validation: Kinetic Monte-Carlo simulations generated 25 $E^*$–$S$ trajectories with experimentally derived underlying state values (based on data in Figure 5) provided in Table 1. Added Gaussian noise ($\sigma_{E^*}=0.025$; $\sigma_S=0.025$) obscured the underlying $E^*$ and $S$ state sequences. Each simulated trajectory contained 1200 data points at 25 ms temporal resolution. Simulations included photobleaching of the 10 bp acceptor, in which the photobleaching time constant was 20 s. Once the 10 bp acceptor photobleached, the transition probabilities (and hence mean dwell times) of the donor-only and 19 bp acceptor states were updated to reflect the removal of kinetic pathways associated with 10 bp acceptor activation. Weighted averaging of state values at transition points accounted for asynchrony between the onset of a state transition and camera integration time. Linked HMM analysis of simulated trajectories proceeded as described above; additionally, a minimum dwell threshold criterion of four data points removed spurious states arising from asynchronous detection, and hence removed transient states similar to states V–VI in Figure 5. By concatenating all simulated trajectories and performing linked HMM, global analysis (accounting for transition artifacts arising from concatenation) accompanied individual linked HMM of each simulated trajectory.

Analysis of individual simulated trajectories, as well as global analysis, revealed strong agreement between simulation input and linked HMM results. Four performance metrics validated linked HMM: a) correct number of inferred states, b) percentage correspondence between simulated state trajectory and linked HMM trajectory, c) percentage false negative transitions, and d) percentage false positive transitions. Linked HMM found 76% of the simulated trajectories to have four states (see Table 1 for mean state values), and the remaining 24% six states. This discrepancy is attributed to false assignment of the 10 bp-acceptor FRET value ($E^*=0.79$) to the slightly different FRET value of the state with both active acceptors ($E^*=0.82$), and vice versa. The error occurred only for short state dwells ($<7$ frames) when the number of data points was insufficient to reliably distinguish the small difference in FRET.

Metrics b–d further validated those trajectories found to have the correct number of inferred states. The linked HMM trajectory corresponded to the underlying simulated state trajectory for 99.51% of frames, that is, linked HMM is capable of correctly identifying the onset and end of individual state dwells. The percentage of false negative transitions of $<5\%$ indicates the sensitivity of the algorithm to individual transitions. The percentage of false positive transitions of less than 1%, demonstrates high specificity of the algorithm. Performance across all metrics can, however, be further enhanced by optimal tuning of switching rates relative to rate of data acquisition and careful planning of relative fluorophore positions $E^*$ and excitation intensities $S$.

## Acknowledgements

*We thank Max Little for kindly providing the step-filter code. S.U., K.G., G.E., and A.N.K. were supported by a UK Bionanotechnology Interdisciplinary Research Collaboration grant, Engineering and Physical Science Research Council grant EP/D058775, and the European Union's Seventh Framework Programme (FP7/2007–2013) under grant agreement n° 201418 (READNA). S.U. was supported by Mathworks. G.E. was supported by the Life Sciences Interface Doctoral Training Centre at Oxford.*

**Keywords:** biophysics · fluorescence · FRET · photophysics · single-molecule studies

[1] X. S. Xie, H. P. Lu, *J. Biol. Chem.* **1999**, *274*, 15967 – 15970.
[2] B. P. English, W. Min, A. M. van Oijen, K. T. Lee, G. Luo, H. Sun, B. J. Cherayil, S. C. Kou, X. S. Xie, *Nat. Chem. Biol.* **2006**, *2*, 87 – 94.
[3] A. N. Kapanidis, T. Strick, *Trends Biochem. Sci.* **2009**, *34*, 234 – 243.
[4] S. V. Solomatin, M. Greenfeld, S. Chu, D. Herschlag, *Nature* **2010**, *463*, 681 – 684.
[5] Y. Santoso, C. M. Joyce, O. Potapova, L. Le Reste, J. Hohlbein, J. P. Torella, N. D. F. Grindley, A. N. Kapanidis, *Proc. Natl. Acad. Sci. USA* **2010**, *107*, 715 – 720.
[6] S. Uemura, C. E. Aitken, J. Korlach, B. A. Flusberg, S. W. Turner, J. D. Puglisi, *Nature* **2010**, *464*, 1012 – 1017.
[7] D. S. Tawfik, *Nat. Chem. Biol.* **2010**, *6*, 692 – 696.
[8] T. Förster, *Ann. Phys.* **1948**, *437*, 55 – 75.
[9] T. Ha, T. Enderle, D. F. Ogletree, D. S. Chemla, P. R. Selvin, S. Weiss, *Proc. Natl. Acad. Sci. USA* **1996**, *93*, 6264 – 6268.
[10] P. R. Selvin, *Nat. Struct. Biol.* **2000**, *7*, 730 – 734.
[11] A. N. Kapanidis, N. K. Lee, T. A. Laurence, S. Doose, A. Margeat, S. Weiss, *Proc. Natl. Acad. Sci. USA* **2004**, *101*, 8936 – 8941.
[12] V. Mekler, E. Kortkhonjia, J. Mukhopadhyay, J. Knight, A. Revyakin, A. N. Kapanidis, W. Niu, Y. W. Ebright, R. Levy, R. H. Ebright, *Cell* **2002**, *108*, 599 – 614.
[13] J. Andrecka, R. Lewis, F. Brückner, E. Lehmann, P. Cramer, J. Michaelis, *Proc. Natl. Acad. Sci. USA* **2008**, *105*, 135 – 140.
[14] A. Muschielok, J. Andrecka, A. Jawhari, F. Brückner, P. Cramer, *J. Michaelis Nat. Methods* **2008**, *5*, 965 – 971.
[15] A. K. Wozniak, G. F. Schröder, H. Grubmüller, C. A. M. Seidel, F. Oesterhelt, *Proc. Natl. Acad. Sci. USA* **2008**, *105*, 18337 – 18342.
[16] S. Hohng, C. Joo, T. Ha, *Biophys. J.* **2004**, *87*, 1328 – 1337.
[17] N. K. Lee, A. N. Kapanidis, H. R. Koh, Y. Korlann, S. O. Ho, Y. Kim, N. Gassman, S. K. Kim, S. Weiss, *Biophys. J.* **2007**, *92*, 303 – 312.
[18] I. Rasnik, S. A. McKinney, T. Ha, *Nat. Methods* **2006**, *3*, 891 – 893.
[19] J. Vogelsang, R. Kasper, C. Steinhauer, B. Person, M. Heilemann, M. Sauer, P. Tinnefeld, *Angew. Chem.* **2008**, *120*, 5545 – 5550; *Angew. Chem. Int. Ed.* **2008**, *47*, 5465 – 5469.
[20] E. Margeat, A. N. Kapanidis, P. Tinnefeld, Y. Wang, J. Mukhopadhyay, R. H. Ebright, S. Weiss, *Biophys. J.* **2006**, *90*, 1419 – 1431.
[21] S. Liu, E. A. Abbondanzieri, J. W. Rausch, S. F. J. Le Grice, X. Zhuang, *Science* **2008**, *322*, 1092 – 1097.
[22] R. Roy, A. G. Kozlov, T. M. Lohman, T. Ha, *Nature* **2009**, *461*, 1092 – 1097.
[23] S. Uphoff, S. J. Holden, L. Le Reste, J. Periz, S. van de Linde, M. Heilemann, A. N. Kapanidis, *Nat. Methods* **2010**, *7*, 831 – 836.
[24] M. Bates, T. R. Blosser, X. Zhuang, *Phys. Rev. Lett.* **2005**, *94*, 108 101.
[25] M. Heilemann, E. Margeat, R. Kasper, M. Sauer, P. Tinnefeld, *J. Am. Chem. Soc.* **2005**, *127*, 3801 – 3806.

  

[26] J. Vogelsang, T. Cordes, C. Forthmann, C. Steinhauer, P. Tinnefeld, *Proc. Natl. Acad. Sci. USA* **2009**, *106*, 8107 – 8112.
[27] E. Betzig, G. H. Patterson, R. Sougrat, O. W. Lindwasser, S. Olenych, J. S. Bonifacino, M. W. Davidson, J. Lippincott-Schwartz, H. F. Hess, *Science* **2006**, *313*, 1642 – 1645.
[28] M. J. Rust, M. Bates, X. Zhuang, *Nat. Methods* **2006**, *3*, 793 – 795.
[29] M. Heilemann, S. van de Linde, M. Schüttpelz, R. Kasper, B. Seefeldt, A. Mukherjee, P. Tinnefeld, M. Sauer, *Angew. Chem.* **2008**, *120*, 6266 – 6271; *Angew. Chem. Int. Ed.* **2008**, *47*, 6172 – 6176.
[30] M. Heilemann, P. Tinnefeld, G. S. Mosteiro, M. G. Parajo, N. F. van Hulst, M. Sauer, *J. Am. Chem. Soc.* **2004**, *126*, 6514 – 6515.
[31] S. Lee, J. Lee, S. Hohng, *PLoS One* **2010**, *5*, e12270.
[32] N. K. Lee, A. N. Kapanidis, Y. Wang, X. Michalet, J. Mukhopadhyay, R. H. Ebright, S. Weiss, *Biophys. J.* **2005**, *88*, 2939 – 2953.
[33] P. R. Selvin, T. Ha, *Single Molecule Techniques: A Laboratory Manual*. Cold Spring Harbor Laboratory Press, Cold Spring Harbor, **2007**.
[34] G. T. Dempsey, M. Bates, W. E. Kowtoniuk, D. R. Liu, R. Y. Tsien, X. Zhuang, *J. Am. Chem. Soc.* **2009**, *131*, 18192 – 18193.
[35] T. Cordes, J. Vogelsang, P. Tinnefeld, *J. Am. Chem. Soc.* **2009**, *131*, 5018 – 5019.
[36] M. Heilemann, S. van de Linde, A. Mukherjee, M. Sauer, *Angew. Chem.* **2009**, *121*, 7036 – 7041; *Angew. Chem. Int. Ed.* **2009**, *48*, 6903 – 6908.
[37] J. Ross, P. Buschkamp, D. Fetting, A. Donnermeyer, C. M. Roth, P. Tinnefeld, *J. Phys. Chem. B* **2007**, *111*, 321 – 326.
[38] M. A. Little, N. S. Jones, IEEE International Conference on Acoustics, *Speech and Signal Processing* **2010**, 4162 – 4165.
[39] S. A. McKinney, C. Joo, T. Ha, *Biophys. J.* **2006**, *91*, 1941 – 1951.
[40] T. H. Lee, *J. Phys. Chem. B* **2009**, *113*, 11535 – 11542.
[41] S. Jung, R. M. Dickson, *J. Phys. Chem. B* **2009**, *113*, 13886 – 13890.
[42] J. E. Bronson, J. Fei, J. M. Hofman, R. L. Gonzalez, C. H. Wiggins, *Biophys. J.* **2009**, *97*, 3196 – 3205.
[43] Y. Liu, J. Park, K. A. Dahmen, Y. R. Chemla, T. Ha, *J. Phys. Chem. B* **2010**, *114*, 5386 – 5403.
[44] K. Gryte, S. Uphoff, A. N. Kapanidis, unpublished results.
[45] J. Hohlbein, K. Gryte, M. Heilemann, A. N. Kapanidis, *Phys. Biol.* **2010**, *7*, 031001.
[46] H. S. Chung, J. M. Louis, W. A. Eaton, *Proc. Natl. Acad. Sci. USA* **2009**, *106*, 11837 – 11844.
[47] S. J. Holden, S. Uphoff, J. Hohlbein, D. Yadin, L. Le Reste, O. J. Britton, A. N. Kapanidis, *Biophys. J.* **2010**, *99*, 3102 – 3111.
[48] S. van de Linde, S. Wolter, M. Heilemann, M. Sauer, *J. Biotechnol.* **2010**, *149*, 260 – 266.
[49] L. A. Rabiner, *Proceedings of the IEEE* **1989**, *77*, 257 – 286.
[50] A. Viterbi, *IEEE Trans. Inf. Theory* **1967**, *13*, 260 – 269.

Received: October 6, 2010
Published online on January 30, 2011

  